Negative Baryon density and the Folding structure of the B=3 Skyrmion

David Foster‡ and Steffen Krusch§

School of Mathematics, Statistics and Actuarial Science,
University of Kent, Canterbury CT2 7NF, United Kingdom

Abstract. The Skyrme model is a non-linear field theory whose solitonic solutions, once quantised, describe atomic nuclei. The classical static soliton solutions, so-called Skyrmions, have interesting symmetries and can only be calculated numerically. Mathematically, these Skyrmions can be viewed as maps between two three-manifolds and, as such, their stable singularities can only be folds, cusps and swallowtails. Physically, the occurrence of singularities is related to negative baryon density. In this paper, we calculate the charge three Skyrmion to a high resolution in order to examine its singularity structure in detail. Thereby, we explore regions of negative baryon density. We also discuss how the negative baryon density depends on the pion mass.

‡ df211@kent.ac.uk
§ S.Krusch@kent.ac.uk

1. Introduction

The Skyrme model is a $(3+1)$-dimensional nonlinear theory of pions and was conjectured by Skyrme as a model of baryons [1]. In 1983, Witten stimulated a surge in research activity by relating the Skyrme model to QCD – in the large colour limit [2]. The minimum-energy solutions of the model are called Skyrmions and, once quantised, are identified as baryons.‖ In this article we are interested in static solutions of the Skyrme model, best defined by the static energy functional

$$E = \frac{1}{12\pi^2} \int \left\{ -\frac{1}{2}\mathrm{Tr}(R_iR_i) - \frac{1}{16}\mathrm{Tr}([R_i, R_j][R_i, R_j]) + m^2\mathrm{Tr}(I_2 - U) \right\} d^3x, \tag{1.1}$$

where $R_\mu = (\partial_\mu U)U^\dagger$ is an $su(2)$ Lie algebra-valued current, and $U(\mathbf{x}, t)$ is an $SU(2)$ Lie group-valued scalar field. The parameter m is related to the physical pion mass m_π via $m = 2m_\pi/(eF_\pi)$ where F_π is the pion decay constant and e is the Skyrme constant. Here we have presented the energy functional in so-called Skyrme-units, see [6, 7] for the "standard values" and [8, 9] for a more detailed discussion of our current understanding. For non-zero pion mass the finite energy requirement forces the field $U : \mathbb{R}^3 \to \mathrm{SU}(2)$ to satisfy

$$\lim_{r \to \infty} U = I_2,$$

and we choose the same boundary condition for $m_\pi = 0$. This one-point compactifies $\mathbb{R}^3$ to the 3-sphere S^3. Using the fact that the group manifold of $\mathrm{SU}(2)$ is also S^3 the field can be extended to a map $U : S^3 \to S^3$. All finite energy field configurations $U(\mathbf{x})$ belong to an element of $\pi_3(S^3) = \mathbb{Z}$, and hence have an associated integer $B \in \mathbb{Z}$. It is this B which is identified as the baryon number and can be explicitly calculated as

$$B = -\frac{1}{24\pi^2} \int \varepsilon_{ijk}\mathrm{Tr}(R_iR_jR_k)d^3x, \tag{1.2}$$
$$= \frac{1}{2\pi^2} \int \det\left(J(\mathbf{x})\right)d^3x,$$

where $J(\mathbf{x})$ is the Jacobian of the map [10]. Naively, the density of B could be assumed to be positive for all $\mathbf{x} \in \mathbb{R}^3$, but this does not have to be the case. It was argued in [11] that as $\mathbb{R}^3$ covers S^3 – the group manifold of $SU(2)$ – there is a folding structure. On these folds the Jacobian-determinant becomes zero which results in tubes of zero baryon density. Inside these tubes singularity theory predicts regions of negative baryon density, but this was never observed in numerical calculations of the full field equations, without imposing any symmetries. This is what we are interested in this paper. It is useful to define two

‖ The quantisation of Skyrmions is the subject of much ongoing research. While semi-classical quantisation has had some recent successes, see e.g. [3], there are also problems with this approach. For example quantum corrections (see e.g. [4] for a detailed discussion) do not necessarily cancel when comparing different sectors [5]. A full discussion of quantisation issues goes beyond the scope of this paper which focuses on classical solutions in the Skyrme model.

quantities,

$$\mathcal{B}_+(x) = \frac{1}{2\pi^2} \max\{\det(J(\mathbf{x})), 0\}, \tag{1.3}$$

$$\mathcal{B}_-(x) = \frac{1}{2\pi^2} \max\{-\det(J(\mathbf{x})), 0\},$$

where $B = \int \mathcal{B}(\boldsymbol{x}) d^3 x$ and trivially $\mathcal{B}(\mathbf{x}) = \mathcal{B}_+(\mathbf{x}) - \mathcal{B}_-(\mathbf{x})$. We refer to these quantities as the positive baryon density and negative baryon density, respectively. Furthermore, the *total* negative baryon density is defined as

$$B_- = \int \mathcal{B}_-(\boldsymbol{x}) d^3 x \tag{1.4}$$

and measures how much negative baryon density occurs in a given field configuration.

The paper is laid out as follows. Section 2 reviews the geometric formulation of the Skyrme model proposed in [10] and discusses the Jacobian. In particular, we show an important identity relating the Jacobian of the Skyrme field to a simpler quantity. Section 3 reviews the rational map ansatz [12] as well as the non-holomorphic rational map ansatz [11]. In section 4 we examine the folding structure of the $B = 3$ Skyrmion using both full field simulation and the non-holomorphic rational map ansatz. Section 4.1 discusses the effects of the pion mass term on the folding structure. In section 4.2 we locally expand the pion fields around the origin and reproduce the singular surface. We end with a conclusion.

2. Geometric setting for Skyrmions

Instead of considering the Skyrme model in a physical field theoretic setting, it can be very insightful to consider it geometrically [10, 13]. In the following, we give a brief account of this approach and set up our notation.

A field configuration is a map $\boldsymbol{\pi}$ from a physical space $\mathbb{R}^3$ to a target space $SU(2)$. Physical space $\mathbb{R}^3$ and target space $SU(2) \cong S^3$ both are 3-dimensional, connected and orientable Riemannian manifolds. Here we choose the Kronecker delta δ_{ij} as the flat-metric on $\mathbb{R}^3$ and $\gamma_{\alpha\beta}$ as the metric on S^3. We denote a point in $\mathbb{R}^3$ as $\mathbf{x}$ and a point in S^3, the image of $\mathbf{x}$, as $\boldsymbol{\pi}(\mathbf{x})$. As $\mathbb{R}^3$ is flat we trivially choose its dreibein to be δ_{ij}, and we choose $\zeta_\mu{}^\alpha(\boldsymbol{\pi}(\mathbf{x}))$ as the dreibein on S^3 with

$$\zeta_\mu{}^\alpha \zeta_\nu{}^\beta \gamma_{\alpha\beta} = \delta_{\mu\nu}. \tag{2.5}$$

Note the inverse of $\zeta_\mu{}^\alpha$ is $\zeta^\mu{}_\alpha$, i.e. $\zeta^\mu{}_\alpha \zeta_\nu{}^\alpha = \delta^\mu{}_\nu$ and $\zeta^\mu{}_\alpha \zeta_\mu{}^\beta = \delta_\alpha{}^\beta$.

Now we can define the Jacobian matrix associated with the map $\boldsymbol{\pi}(\mathbf{x})$ as

$$J_i{}^\mu(\mathbf{x}) = (\partial_i \pi^\alpha(\mathbf{x})) \zeta^\mu{}_\alpha(\boldsymbol{\pi}(\mathbf{x})). \tag{2.6}$$

The matrix $J_i{}^\mu(\mathbf{x})$ is a measure of the deformation induced by the map $\boldsymbol{\pi}$ at the point $\mathbf{x}$ in $\mathbb{R}^3$. We can define a useful quantity called the strain tensor D_{ij}, as

$$D_{ij}(\mathbf{x}) = J_i{}^\mu(\mathbf{x}) J_j{}^\nu(\mathbf{x}) \delta_{\mu\nu} = (\partial_i \pi^\alpha(\mathbf{x}))(\partial_j \pi^\beta(\mathbf{x})) \gamma_{\alpha\beta}. \tag{2.7}$$

3

The strain tensor is invariant under rotations in target space (i.e. rotations of the frame fields $\zeta_\mu{}^\alpha(\boldsymbol{\pi}(\mathbf{x}))$), but not under orthogonal rotations of the physical space $\mathbb{R}^3$. But it is well known that the characteristic polynomial $P = \det(D - \lambda I_3)$ is invariant under rotations. So, we can now define the three invariants,

$$
\begin{aligned}
\mathrm{Tr}(D) &= \lambda_1^2 + \lambda_2^2 + \lambda_3^2, \\
\frac{1}{2}(\mathrm{Tr}(D))^2 - \frac{1}{2}\mathrm{Tr}(D^2) &= \lambda_1^2\lambda_2^2 + \lambda_1^2\lambda_3^2 + \lambda_2^2\lambda_3^2, \\
\det(\mathrm{D}) &= \lambda_1^2\lambda_2^2\lambda_3^2,
\end{aligned}
\tag{2.8}
$$

where $\lambda_1^2, \lambda_2^2, \lambda_3^2$ are the non-negative eigenvalues of the symmetric matrix D_{ij}.

Reparametrising the $SU(2)$-valued field in the traditional way with the three Pauli matrices, τ_a, and the four scalar fields $\sigma(\mathbf{x}), \pi_a(\mathbf{x})$ $(a = 1, 2, 3)$ as

$$
U(\mathbf{x}) = \sigma(\mathbf{x}) + i\boldsymbol{\pi}(\mathbf{x}) \cdot \boldsymbol{\tau},
\tag{2.9}
$$

we see that $\sigma(\mathbf{x})$ and $\boldsymbol{\pi}(\mathbf{x})$ must satisfy the constraint $\sigma^2 + \boldsymbol{\pi} \cdot \boldsymbol{\pi} = 1$ for all $\mathbf{x} \in \mathbb{R}^3$. As pointed out in [13], $\pi^\alpha(\mathbf{x})$ in the above geometric discussion can be identified with the vector π_a in (2.9) and $\sigma(\mathbf{x})$ is a function of $\pi_a(\mathbf{x})$ which ensures that $U(\mathbf{x}) \in SU(2)$. Now, we can define the induced-metric on S^3 as

$$
\gamma_{\alpha\beta}(\mathbf{x}) = \delta_{\alpha\beta} + \frac{\pi_\alpha \pi_\beta}{\sigma^2}.
$$

A short calculation in [13] shows that

$$
D_{ij}(\mathbf{x}) = -\frac{1}{2}\mathrm{Tr}(R_i R_j),
$$

and the energy functional (1.1) can be rewritten as

$$
\begin{aligned}
E &= \mathrm{Tr}(D) + \frac{1}{2}(\mathrm{Tr}(D))^2 - \frac{1}{2}\mathrm{Tr}(D^2), \\
&= \lambda_1^2 + \lambda_2^2 + \lambda_3^2 + \lambda_1^2\lambda_2^2 + \lambda_1^2\lambda_3^2 + \lambda_2^2\lambda_3^2.
\end{aligned}
\tag{2.10}
$$

Also, it is easy to see from the above relations that the baryon number integral (1.2) can be written in terms of these eigenvalues as

$$
B = \frac{1}{2\pi^2}\int \lambda_1 \lambda_2 \lambda_3 \, d^3x.
\tag{2.11}
$$

2.1. The Jacobian

In the following we calculate the Jacobian in stereographic coordinates. This is needed for the analysis of the numerically found solutions. Consider the Skyrme field in sigma model coordinates $(\sigma(\mathbf{x}), \pi_i(\mathbf{x}))$ with $\sigma^2 + \boldsymbol{\pi}^2 = 1$. Then we can define stereographic coordinates by projecting from the North pole N $(\sigma = 1)$ as

$$
\Phi_N^\alpha = \frac{\pi^\alpha}{1 - \sigma}.
\tag{2.12}
$$

Note that the metric in stereographic coordinates for this chart is given by

$$ds_N^2 = \sum_{\alpha=1}^{3} \frac{4}{(1+R_N{}^2)^2} (d\Phi_N^\alpha)^2 , \tag{2.13}$$

where $R_N{}^2 = \sum_{\alpha=1}^{3} (\Phi_N^\alpha)^2 = \frac{1+\sigma}{1-\sigma}$. Since the metric (2.13) is diagonal we can define the frame fields

$$\zeta_{N\mu}{}^\alpha = \frac{1+R_N{}^2}{2} \delta_\mu{}^\alpha \quad \text{and its inverse} \quad \zeta_N{}^\mu{}_\alpha = \frac{2}{1+R_N{}^2} \delta^\mu{}_\alpha. \tag{2.14}$$

Hence, the components of the Jacobian matrix J_N are given by

$$J_{Nm}{}^\mu = \frac{\partial \Phi_N^\alpha}{\partial x_m} \zeta_N{}^\mu{}_\alpha = \frac{\partial \Phi_N^\mu}{\partial x_m} \frac{2}{1+R_N{}^2}. \tag{2.15}$$

Using (2.7) we can calculate the strain tensor D_{mn} and obtain

$$D_{Nmn} = \frac{4}{(1+R_N{}^2)^2} \frac{\partial \Phi_N^\alpha}{\partial x_m} \frac{\partial \Phi_N^\beta}{\partial x_n} \delta_{\alpha\beta}. \tag{2.16}$$

Note 'N' is not an index to be summed over.

To obtain a well-defined $SO(3)$ frame bundle the frame fields ζ_S have to be chosen as

$$\zeta_{S\mu}{}^\alpha = -\frac{1+R_S^2}{2} \delta_\mu{}^\alpha \quad \text{and its inverse.} \tag{2.17}$$

See e.g. [14] for further details. This leads to

$$J_{Sm}{}^\mu = -\frac{\partial \Phi_S^\mu}{\partial x_m} \frac{2}{1+R_S^2}, \tag{2.18}$$

where $\Phi_S^\alpha = \frac{\pi^\alpha}{1+\sigma}$ is the South pole projection.

The minus sign in (2.18) arises because stereographic coordinates are related by inversion, which has negative determinant. The expression for the strain tensor D_{Smn} is

$$D_{Smn} = \frac{4}{(1+R_S^2)^2} \frac{\partial \Phi_S^\alpha}{\partial x_m} \frac{\partial \Phi_S^\beta}{\partial x_n} \delta_{\alpha\beta} \tag{2.19}$$

There is a sign ambiguity when defining the Jacobians J_N and J_S. Here we have chosen the Jacobian such that the standard hedgehog has positive Jacobian. In fact, for $B = 1$ the hedgehog can be written as

$$\sigma = \cos(f(r)) \quad \text{and} \quad \pi_i = \frac{x_i}{r} \sin(f(r)), \tag{2.20}$$

where $r = \sqrt{x_1^2 + x_2^2 + x_3^2}$ and f is a real radial shape function that can be determined numerically. Asymptotically, $f(r) \approx \pi - Ar$ as $r \to 0$ with $A > 0$ and $f(r) \approx \frac{C}{r^2}$ as $r \to \infty$ with $C \approx 2.16$, see e.g. [15]. Near the origin, $\sigma \approx -1$, so we project from the north pole and obtain $\det J_N \approx A^3 > 0$, whereas as $r \to \infty$, $\sigma \approx 1$ we project from the south pole and $J_S \approx \frac{2C^3}{r^9} > 0$. These expression of the Jacobians (J_N and J_S) are useful when examining the

behaviour near the north and south pole, which corresponds to the vacuum $\sigma = 1$ and the anti-vacuum $\sigma = -1$ respectively.¶

For analysis of numerical data later in the paper, we can express the Jacobian directly in terms of the four pion fields as

$$J_{Nm}{}^\mu = (1 - \sigma)\frac{\partial \Phi_N{}^\mu}{\partial x_m} \tag{2.21}$$

$$= \frac{\partial \pi^\mu}{\partial x_m} + \frac{\pi^\mu}{(1 - \sigma)}\frac{\partial \sigma}{\partial x_m} \tag{2.22}$$

$$= \frac{\partial \pi^\mu}{\partial x_m} - \sum_\nu \frac{\pi^\mu \pi^\nu}{\sigma(1 - \sigma)}\frac{\partial \pi^\nu}{\partial x_m}, \tag{2.23}$$

where we used the identity

$$\sigma\frac{\partial \sigma}{\partial x_j} = -\sum_{\nu=1}^{3} \pi^\nu \frac{\partial \pi^\nu}{\partial x_j}, \tag{2.24}$$

which is derived by differentiating the normalisation condition.

As a check, we can evaluate

$$D_{mn} = J_m{}^\mu(x)J_n{}^\nu(x)\delta_{\mu\nu} \tag{2.25}$$

and obtain

$$D_{mn} = \frac{\partial \pi^\mu}{\partial x_m}\frac{\partial \pi^\nu}{\partial x_n}\left(\delta_{\mu\nu} - \frac{\pi_\mu \pi_\nu}{\sigma^2}\right). \tag{2.26}$$

The term in the brackets corresponds to the induced metric in (σ, π_i) coordinates. Using the identity (2.24) we obtain the more familiar expression

$$D_{mn} = \frac{\partial \sigma}{\partial x_m}\frac{\partial \sigma}{\partial x_n} + \frac{\partial \pi^\mu}{\partial x_m}\frac{\partial \pi^\nu}{\partial x_n}\delta_{\mu\nu}. \tag{2.27}$$

With this expression, equation (2.10) gives the pion field version of the Skyrme Lagrangian which is often used for numerical simulations, see e.g. [16]. It can be shown by direct calculation that

$$\det(J_N) = -\det(J_0)/\sigma, \tag{2.28}$$

where the components of the unframed Jacobian matrix J_0 is given by

$$J_{0ji} = \frac{\partial \pi_i}{\partial x_j}. \tag{2.29}$$

Hence $\det J_N$ vanishes when $\det J_0$ does for $\sigma \neq 0$, therefore J_N and J_0 have the same singular surfaces. Equation (2.28) is useful in section 4.2 when discussing the folding structure of $B = 3$.

¶ Here, vacuum and anti-vacuum refers to the absence of pion fields. Vacuum and anti-vacuum are antipodal points when viewing the target space $SU(2)$ as a 3-sphere. For massless pions, $m = 0$, any constant field has zero energy (1.1), yet for massive pions, $m > 0$, the vacuum $\sigma = 1$ is the unique configuration with zero energy.

3. Rational map ansatz

The rational map ansatz[+] [12] makes use of the feature that a point in $\mathbb{R}^3$ can be written in polar coordinates (r, z) where the angular coordinate z is represented by a point on the Riemann sphere via $z = e^{i\phi} \tan \frac{\theta}{2}$. The Skyrme field $U(\mathbf{x})$ then takes the form

$$U(r, z) = \exp(if(r)\boldsymbol{n}(z) \cdot \boldsymbol{\tau}), \tag{3.30}$$

where $f(r)$ is a real valued profile function with the boundaries $f(0) = \pi$ and $f(\infty) = 0$; $\boldsymbol{\tau} = (\tau_1, \tau_2, \tau_3)$ is the triplet of Pauli matrices and $\boldsymbol{n}$ is the unit vector

$$\boldsymbol{n}(z) = \frac{1}{1 + |R(z)|^2}(R(z) + \overline{R(z)}, i(\overline{R(z)} - R(z)), 1 - |R(z)|^2).$$

$R(z)$ is a holomorphic rational map between Riemann spheres, and is given by the two polynomials $p(z), q(z)$,

$$R(z) = \frac{p(z)}{q(z)}.$$

Then the baryon number is equal to the algebraic degree of $R(z)$,

$$\deg(R(z)) = \max\{\deg(p(z)), \deg(q(z))\}.$$

Such a field configuration is a suspension and gives rise to an isomorphism between $\pi_3(S^3)$ and $\pi_2(S^2)$. This point of view proved very useful for quantising Skyrmions in [17] because a suspension provides a natural way to calculate homotopy groups of the Skyrmion configuration space from the space of rational maps. It is the choice of $R(z)$ which replicates the polyhedral shape of Skyrmions, and the symmetries of the accepted numerical solutions. The benefit of the rational map ansatz is that it gives rise to the following three simple eigenvalues of the strain tensor,

$$\lambda_1 \quad = -f'(r) \tag{3.31}$$
$$\lambda_2 = \lambda_3 = \frac{\sin f}{r} \frac{1 + |z|^2}{1 + |R|^2} \left| \frac{dR}{dz} \right|.$$

Inserting these eigenvalues into equation (2.10) gives the simple radial energy functional

$$E = 4\pi \int \left(f'^2 r^2 + 2B(f'^2 + 1)\sin^2 f + \mathcal{I}\frac{\sin^4 f}{r^2} + 2m^2 r(1 - \cos f) \right) dr, \tag{3.32}$$

where

$$\mathcal{I} = \frac{1}{4\pi} \int \left(\frac{1 + |z|^2}{1 + |R|^2} \left| \frac{dR}{dz} \right| \right)^4 \frac{2i\,dz\,d\bar{z}}{(1 + |z|^2)^2}. \tag{3.33}$$

[+] Technically, this is not an *ansatz* but rather an *approximation*. It is a very useful tool for obtaining initial configurations for numerical minimisations, and it gives a more fundamental understanding of the symmetries of Skyrmions. However, since this term is widely used in the literature we will also refer to the rational map approximation as the rational map ansatz.

This energy functional can be easily minimised by choosing the correct degree polynomials $p(z), q(z)$ which minimise $\mathcal{I}$, then numerically minimising the profile function $f(r)$. The minimum energy solutions found using this method only exceed the non-symmetry numerical solutions by about 3%, see e.g. [12, 16, 18].

This holomorphic ansatz is very successful at capturing the major features of the Skyrme model and is a very useful technique to give initial configurations which are close to the minimum energy solutions for numerical minimisation. This avoids numerically expensive collisions which were previously used to create appropriate initial conditions [19, 16]. A feature of the holomorphic ansatz is that it locally preserves orientation. Hence there cannot be regions of negative baryon density. This constrains the possible configurations. We can extend the ansatz to non-holomorphic $R(z, \bar{z})$ as in [11]. This now allows points in $\mathbb{R}^3$ with negative baryon density. In this case the three eigenvalues of the strain tensor D_{ij} are slightly more complicated and are

$$\lambda_1 = -f'(r), \tag{3.34}$$
$$\lambda_2 = \frac{\sin f}{r}(|R_z| + |R_{\bar{z}}|)\frac{1 + |z|^2}{1 + |R|^2},$$
$$\lambda_3 = \frac{\sin f}{r}(|R_z| - |R_{\bar{z}}|)\frac{1 + |z|^2}{1 + |R|^2},$$

where R_z and $R_{\bar{z}}$ are the derivatives of R with respect to z and $\bar{z}$, respectively. It is now apparent that for non-holomorphic (or non-antiholomorphic) R the angular strains λ_2, λ_3 are no longer isotropic, and only when R_z (or $R_{\bar{z}}$) equal zero do we regain the previous holomorphic ansatz. The energy functional for this more general ansatz is

$$E = \frac{1}{3\pi} \int \left(f'^2 r^2 + 2\mathcal{J}(f'^2 + 1)\sin^2 f + \tilde{\mathcal{I}}\frac{\sin^4 f}{r^2} + 2m^2 r(1 - \cos f) \right) dr, \tag{3.35}$$

where

$$\mathcal{J} = \frac{1}{4\pi} \int \left((|R_z|^2 + |R_{\bar{z}}|^2)\left(\frac{1 + |z|^2}{1 + |R^2|}\right)^2 \right) \frac{2idzd\bar{z}}{(1 + |z|^2)^2}, \tag{3.36}$$

$$\tilde{\mathcal{I}} = \frac{1}{4\pi} \int \left((|R_z|^2 - |R_{\bar{z}}|^2)\left(\frac{1 + |z|^2}{1 + |R|^2}\right)^2 \right)^2 \frac{2idzd\bar{z}}{(1 + |z|^2)^2}, \tag{3.37}$$

and

$$B = \frac{1}{2\pi} \int f'(r)\sin^2 f(r) \left((|R_z|^2 - |R_{\bar{z}}|^2)\left(\frac{1 + |z|^2}{1 + |R|^2}\right)^2 \right) \frac{2idzd\bar{z}}{(1 + |z|^2)^2}. \tag{3.38}$$

Again $f(r)$ is a profile function which is a solution of the ODE

$$(r^2 + 2\mathcal{J}\sin^2 f)f'' + 2rf' + (\mathcal{J}f'^2 - \mathcal{J} - \tilde{\mathcal{I}}\frac{\sin^2 f}{r^2})\sin 2f - m^2 r\sin f = 0, \tag{3.39}$$

with the boundary conditions $f(0) = \pi$ and $f(\infty) = 0$.

As above, we restrict to maps of the form

$$R(z, \bar{z}) = \frac{p(z, \bar{z})}{q(z, \bar{z})},$$

where the $\bar{z}$ dependence is chosen in such a way as to preserve the symmetry of the original minimal energy rational map. Then the baryon number is generically equal to $N_1 - N_2$, where N_1 is the maximal holomorphic degree of (p, q) and N_2 is the maximal antiholomorphic degree of (p, q).

In (3.39) $\mathcal{J}$ replaces the role of B in the holomorphic rational map ansatz. This has a significant effect on the profile function f. To study this effect we linearise (3.39) about $r = 0$ and set $f(r) = \pi - \nu(r)$ where $\nu(r) \ll 1$. This gives the new linear ODE

$$r^2 \nu'' + 2r\nu' - 2\mathcal{J}\nu + m^2 r\nu = 0, \tag{3.40}$$

with the solution

$$f(r) = \pi - Cr^{\left(\frac{-1 + \sqrt{1 + 8\mathcal{J}}}{2}\right)} + \ldots \tag{3.41}$$

For $m = 0$, equation (3.40) is a Cauchy-Euler equation, whereas for $m \neq 0$ the solution is given in terms of a Bessel function. Numerical calculations show that as the pion mass is increased, $\mathcal{J}$ becomes larger and hence f decays slower about the origin. We can now play the same trick for the limit of r going to infinity. Here we set $f(r) = \epsilon(r)$ where $\epsilon(r) \ll 1$, giving the linearised equation

$$r^2 \epsilon'' + 2r\epsilon' - 2\mathcal{J}\epsilon - m^2 r\epsilon = 0.$$

This gives the solutions

$$f(r) = \begin{cases} Cr^{-\left(\frac{1 + \sqrt{1 + 8\mathcal{J}}}{2}\right)}, & \text{if } m = 0, \\ \frac{Ce^{-2m\sqrt{r}}}{r^{3/4}}\left(1 + \frac{4(1 + 8\mathcal{J}) - 1}{16m\sqrt{r}} + \ldots\right), & \text{if } m \neq 0. \end{cases}$$

The effect of the mass term is to make the solution more localised around the origin.

4. The $B = 3$ Skyrmion

It has been known for a long time that the baryon density for the $B = 3$ Skyrmion is tetrahedrally symmetric [20, 19]. A lot of its features can be explained by a tetrahedrally symmetric rational map [12]. But, as shown in [11], the non-holomorphic rational map allows negative baryon density and has lower energy that the holomorphic map. The non-holomorphic rational map gives rise to four singular tubes $(\det(J) = 0)$ which start at the origin, pass through the faces of the tetrahedron then go off to infinity. It has been shown in [11] that there are three folding lines equally spaced along these tubes. Also, in the centre of these tubes there are regions of negative baryon density. This inspired us to explore the form and amount of negative baryon density in actual minimum-energy Skyrme solutions. The

calculations in [11] were performed for zero pion mass, $m = 0$. Therefore, we first describe the $m = 0$ case and then discuss the effects of non-zero pion mass, $m > 0$, in section 4.1.

The family of rational maps for the $B = 3$ Skyrmion with the correct symmetry is

$$R = \frac{p_1 \cos \chi + p_2 \sin \chi}{q_1 \cos \chi + q_2 \sin \chi}, \tag{4.42}$$

where the polynomials p_1, p_2, q_1 and q_2 are

$$
\begin{aligned}
p_1(z, \bar{z}) &= i\sqrt{3}z^3\bar{z} + i\sqrt{3}z^3 - z\bar{z} - 1, & q_1(z, \bar{z}) &= z^4\bar{z} + z^3 - i\sqrt{3}z^2\bar{z} - i\sqrt{3}z, \\
p_2(z, \bar{z}) &= z^4 - 2i\sqrt{3}z^2 + 1, & q_2(z, \bar{z}) &= -z^4\bar{z} + 2i\sqrt{3}z^2\bar{z} - \bar{z}.
\end{aligned} \tag{4.43}
$$

With a simple numerical scanning algorithm we find that the family of rational maps in (4.42) attains its minimum energy for $\chi = 0.154$. This gives $E/B = 1.161$. Note this is lower than the minimum energy for the holomorphic ansatz ($E/B = 1.184$). This value of χ is slightly lower than that found in [11]. This difference is believed to be due to numerical accuracy.
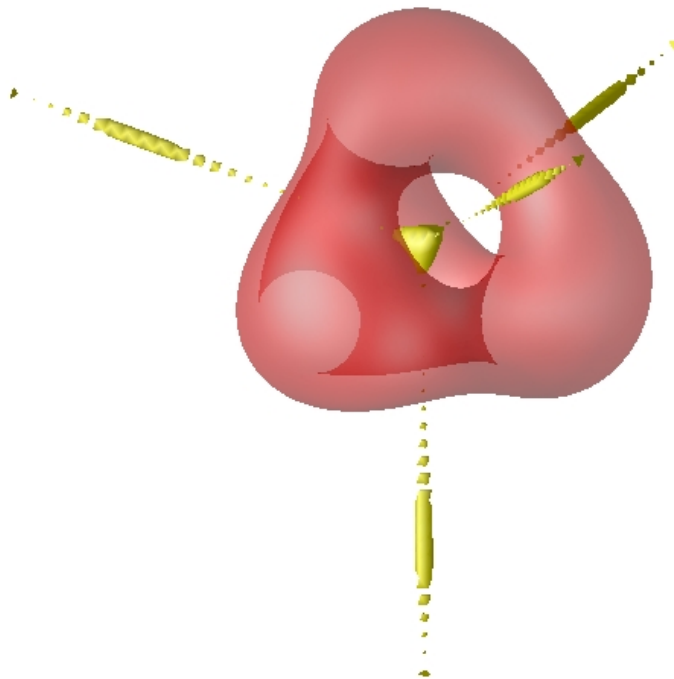

Figure 1: Baryon number three minimum-energy solution for zero pion mass, $m = 0$. The red surface is a level set of constant positive baryon density. The yellow surface is a level set of constant negative baryon density.

To find the $B = 3$ minimum energy solution we numerically minimised this rational map ansatz on a lattice of 250^3 points, with spacing $\Delta x = 0.08$ using fourth order accurate derivatives. For $m = 0$ we find $E/B = 1.146$ and the negative baryon density $B_- = 4.5 \times 10^{-5}$. This is in reasonable agreement with $B_- = 9.25 \times 10^{-5}$ found for the non-holomorphic rational map for $\chi = 0.154$. A surface of constant baryon density (ie. constant Jacobian determinant) is displayed in figure 1 for this solution.

10

To truly capture these regions of negative baryon density we were forced to have a very large box. It is known that asymptotically the $B = 3$ Skyrmion decays as a $B = -1$ Skyrmion [21]. The $B = 1$ Skyrmion can be calculated from the highly symmetric rational map, $R = z$, known as the hedgehog ansatz. Then the equations of motion (3.39) can be linearised to obtain the asymptotic behaviour of the radial profile function $f \sim C/r^2$ as $r \to \infty$ for some constant C. Substituting this into the radial energy-density (3.35) and baryon density (3.38), we find that the energy-density scales as $1/r^4$ and the baryon-density as $1/r^7$. We have checked numerically that choosing $U(\boldsymbol{x}) = I_2$ on the boundary of the numerical box contains the baryon-density within the accuracy of our numerics. However, for an evaluation of the total energy to a high order of accuracy contributions from outside the box need to be included, see e.g. [22] for further details.

Yellow is a level surface of $\det(J(\boldsymbol{x})) \simeq 0$, and red is the surface of the anti-vacuum $\sigma \simeq -1$.

Pre-images of the anti-vacuum. Red is where $\text{sign}(J(\boldsymbol{x})) = -1$, and ivory is where $\text{sign}(J(\boldsymbol{x})) = 1$.
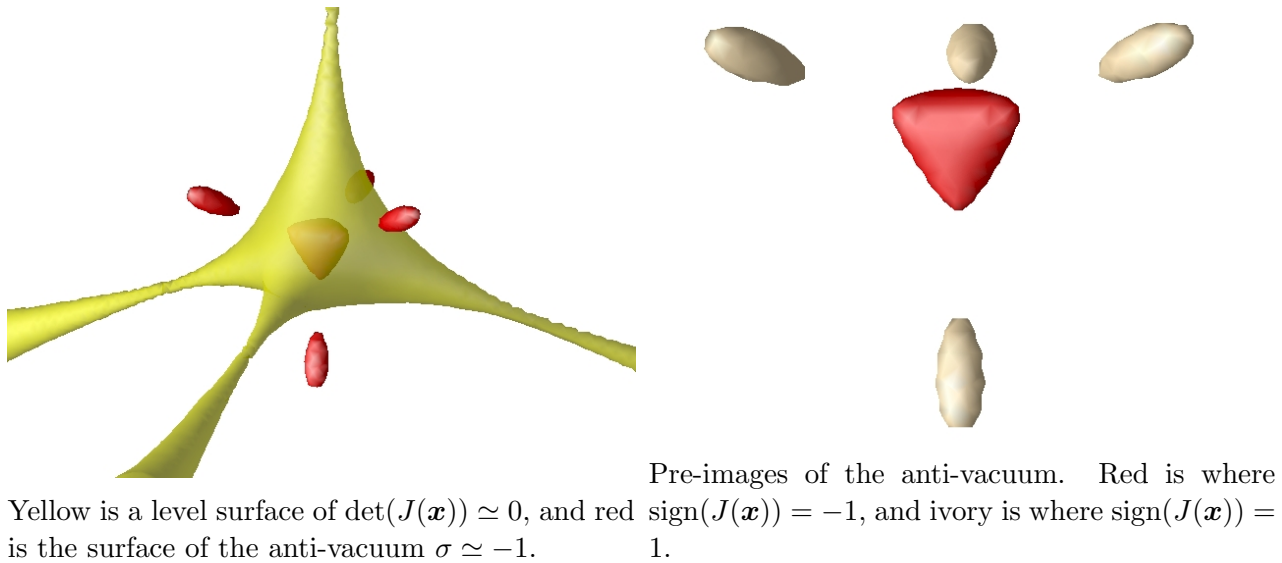
Figure 2: Minimisation of the central region of the $B = 3$ non-holomorphic rational map for zero pion mass, $m = 0$.

Figure 1 shows the regions of negative baryon density of the minimum-energy baryon number three Skyrmion. A point of particular interest is the tetrahedron of negative baryon density in the centre of the Skyrmion. Each of the corners of this dual-tetrahedron gives rise to tubes of $\det(J) = 0$, which pass though the faces of the tetrahedron with positive baryon density. However, the singular surface tubes may or may not be connected to the dual tetrahedron singular surface in the centre. In order to explore how these singular surfaces are connected we performed a numerical simulation over a box centred at the origin with $(\Delta x = 0.01, n = 180)$ sides about 9% of the large box. This is a large increase in resolution, increasing the number of points per unit distance by a factor of 8 in each direction. The boundary conditions, on the surface of the box, are important. One option would be to

11

interpolate the numerical configuration displayed in figure 2. However, due to the large number of additional points such an interpolation is very challenging to calculate and not necessary very reliable. We chose the boundary conditions to be the rational map (4.42) with the minimum-energy profile function found numerically which is a good approximation to the exact solution. The result of our numerical calculation is presented in figure 2 and shows the singularity structure near the origin of the $B = 3$ Skyrmion.

Figure 2a shows the folding tubes in yellow. Contrary to the conjecture in [11] the tubes do not seem to pinch off to singular points. This is evidence that there are no swallowtails in the $B = 3$ Skyrmion and will be discussed further in the next subsection. Figure 2b is also interesting. It shows that it is energetically favourable for the $B = 3$ Skyrmion to 'create' two more pre-images of the anti-vacuum, one with positive orientation and one with negative orientation. The rational map ansatz (3.30) has the anti-vacuum as a suspension point. Hence for the rational map ansatz there are only three pre-images of the vacuum, all at the origin and with positive orientation. The extra pre-images in figure 2b are very similar to the monopole zeros of the Higgs field in [23] where they find five monopole zeros, four positive and one negative. As outlined in [23], one would naively suspect that a positive orientation point would annihilate with a negative orientation point. However, the configuration may be stabilised by tetrahedral symmetry.

4.1. The effects of the pion mass on the folding structure

It is well known that the Skyrme theory describes atomic nuclei better when a pion mass term is included, see [7, 24, 3] for a discussion of $m \neq 0$ and [8] for the implications to spinning Skyrmions. This inspired us to investigate how the surfaces of $\det(J(\boldsymbol{x})) = 0$ vary as a function of m. In this section, we first examine this question using the non-holomorphic rational map ansatz and then check our results using full field minimisation. As a side effect, this analysis provides a good test of the effectiveness of the rational map ansatz.

In order to find the minimum-energy rational map in (4.43) for given m we minimised the numerical integral of (3.35) with respect to χ using a standard search algorithm. The resulting function $\chi(m)$ is displayed in figure 3a for values of m between 0 and 1. The energy per baryon number is shown in figure 3b. Note that E/B increases monotonically as m increases which agrees with the findings in [24]. A point worth noting is that it is energetically favourable for $\tilde{\mathcal{I}}$ to decrease slightly, see figure 3c, and for $\mathcal{J}$ to increase as m increases, see figure 3d. This has an effect on the behaviour of the shape function around the origin as can be seen from equation (3.41).

The radial integral of the baryon density in (3.38) can be evaluated exactly using the boundary conditions of $f(r)$. Using the minimum-energy $\chi(m)$ we then integrated the negative baryon density $\mathcal{B}_-$ over S^2 to give the total negative baryon density B_- as defined in (1.4). Figure 4a shows B_- as a function of m. It is apparent that as the mass m increases it is more energetically efficient for the $B = 3$ Skyrmion to have more negative baryon density, B_-. As shown in figure 4a there is a 40% increase in negative baryon density as m increases
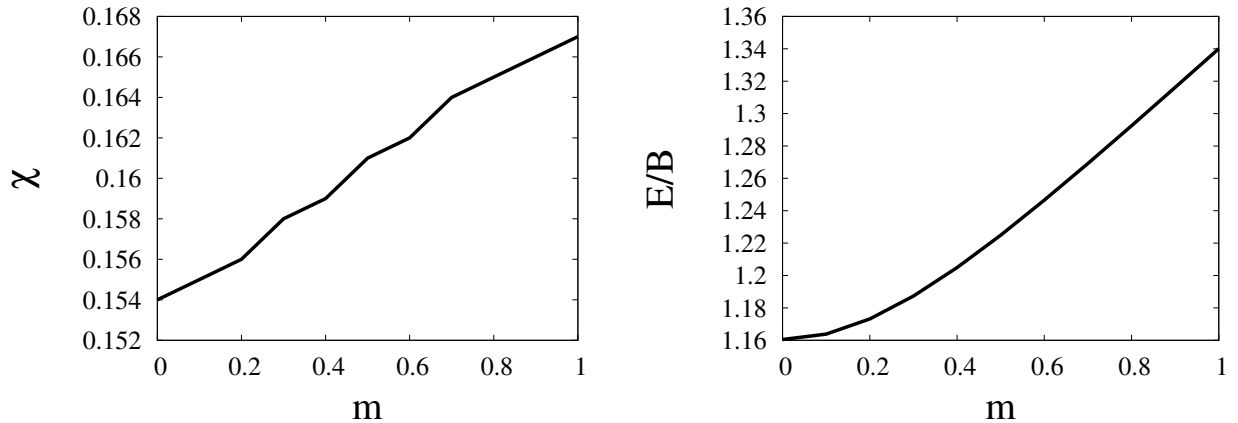
The value of χ which yields the minimum-energy rational map ansatz (4.42).

E/B in (3.35) for the optimal value of χ as a function of m.
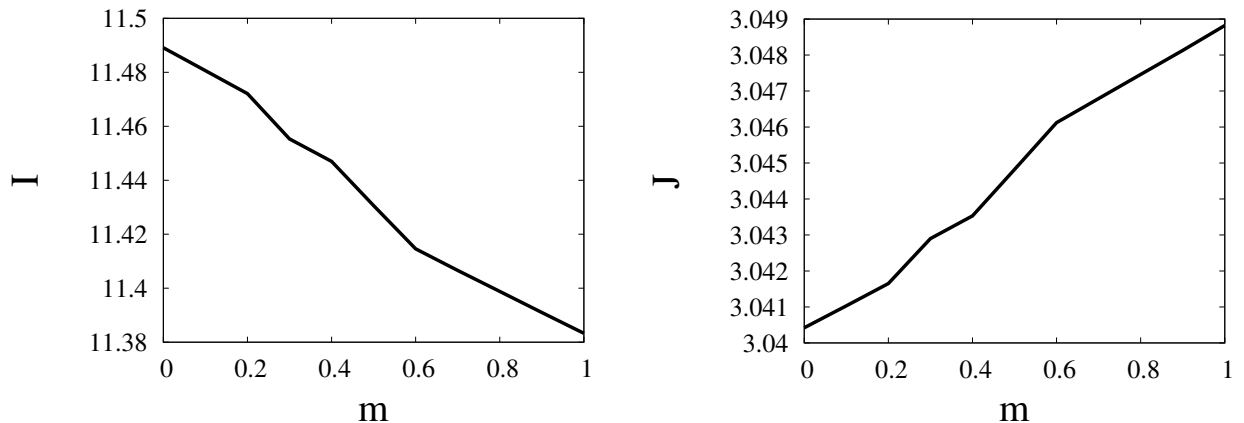
$\tilde{\mathcal{I}}$ in (3.37) for the optimal value of χ as a function of m.

$\mathcal{J}$ in (3.36) for the optimal value of χ as a function of m.

Figure 3: The minimum-energy E/B, $\tilde{\mathcal{I}}$, $\mathcal{J}$ and χ as a function of m.

from 0 to 1.

In the rational map ansatz, the negative baryon density arise as tubes emanating from the faces of the tetrahedral polyhedron, very similar to the yellow tubes in figure 1. To study how these tubes change as a function of mass, we numerically integrated the area of a negative baryon density tube over S^2. This is shown in figure 4b. Hence, the rational map ansatz predicts that the tubes of negative baryon density increase in size roughly linearly with m.

To proceed we used the rational maps for the values of the pion mass given above to generate the initial conditions for a full field minimisation on a square lattice of 250^3 points with lattice spacing $\Delta x = 0.08$, as before. The results are shown in figures 5. It is worth discussing the actual full field minimum-energy $B = 3$ solutions. One should first note that the hole in the level-set of positive $\det(J(x))$ becomes smaller for increasing m. This is

13
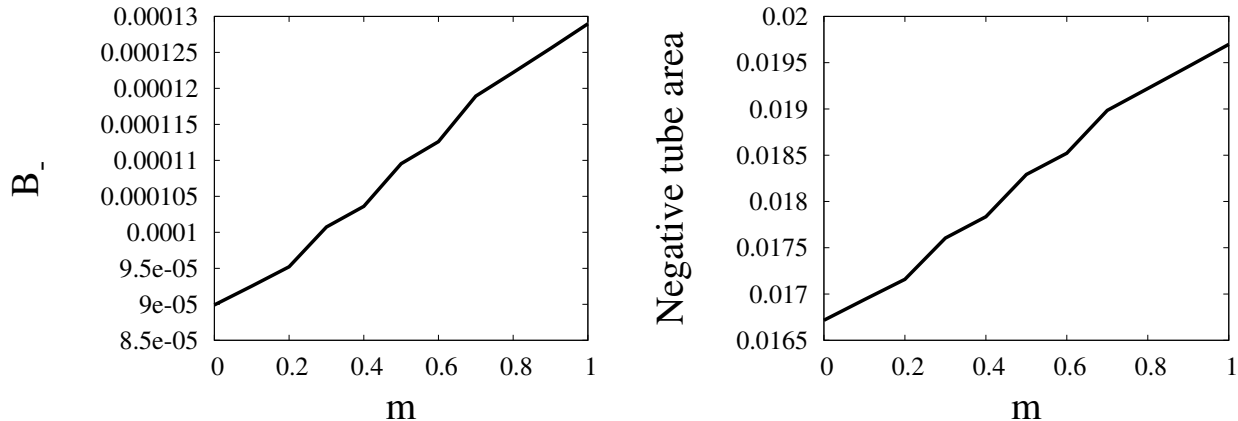
The total negative baryon density B_- (1.4) as a function of m.

Area of the negative baryon density tubes as a function of m.

Figure 4: Data arising from the minimum-energy $B = 3$ rational map (4.42).

well understood as the potential term forces the Skyrmion field to reach the vacuum value exponentially. Also, as m increases the singular tubes become more pronounced. This is clearly seen in figure 5 where the singular tubes are much more defined for $m = 1$ than for $m = 0.1$.

As shown in figure 6a, the energy per baryon for the full field minimisation is about 2% lower than that for the rational map ansatz, for all m. This is expected, because as previously shown the rational map ansatz forces all of the pre-images of the anti-vacuum to be at the origin.

As can be seen in figure 2a the Skyrme field has a fifth pre-image at the origin with negative orientation showing that there is also negative baryon density at the origin. This region of negative baryon density is inside a tetrahedron, which is dual to a surface of positive baryon density. In this central region $\sigma \approx -1$, and this is where the potential energy (the pion mass term) is maximal. Hence as m increase the negative baryon density at the origin decreases. To verify this we numerically integrated over the central tetrahedron of negative baryon density. This is shown in figure 6c where as m increases the total negative baryon density in the central dual tetrahedron decreases. Hence, as the pion mass m increases there are two competing trends. On the one hand, the negative baryon density in the folds increases as in the non-holomorphic rational map ansatz. On the other hand, the negative baryon density at the centre decreases. This gives a heuristic explanation of the behaviour of the total negative baryon density shown in figure 6b. Initially it decreases, as m increases from $m = 0$ to $m \approx 0.7$. Then the negative baryon density starts to increase again. This trend is further verified because we also found the minimum-energy $B = 3$, $m = 2$ solution. This solution has $E/B = 1.551$, $B_- = 4.1 \times 10^{-5}$ and a B_- dual tetrahedron with total baryon density of 1.2×10^{-5}. Figure 6c is not very smooth. This is most likely due to the numerical grid and the algorithm which identified the edge of the dual tetrahedron.
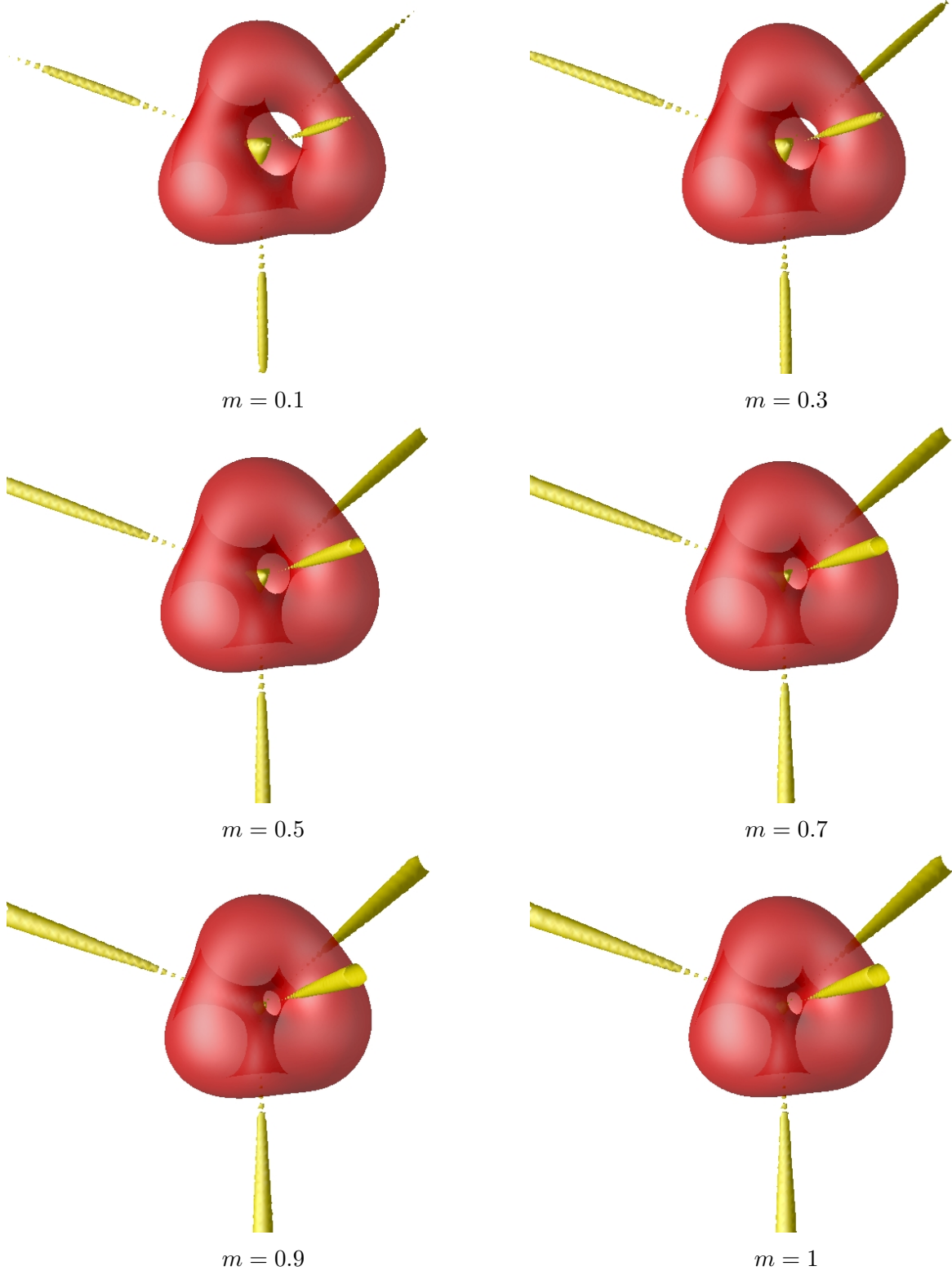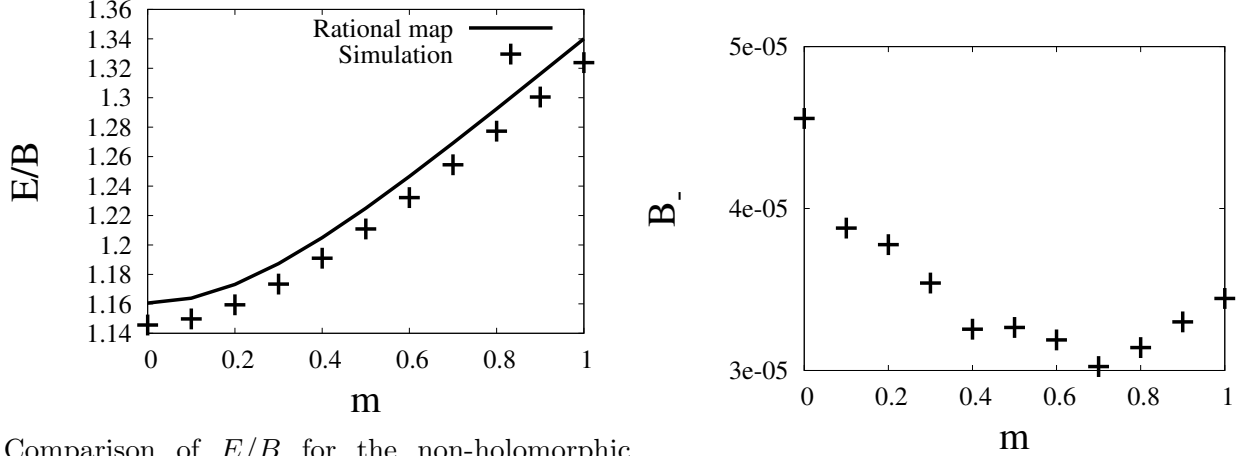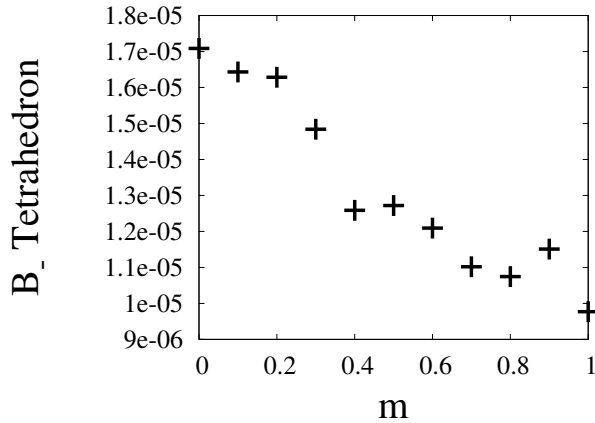
14

$m = 0.1$

$m = 0.3$

$m = 0.5$

$m = 0.7$

$m = 0.9$

$m = 1$

Figure 5: $B = 3$ Skyrmion of varying m. Red is a level set of $B = \text{const} > 0$, yellow is $B = 0$.

Comparison of E/B for the non-holomorphic rational map ansatz and E/B found from full field minimisation as a function of m.

Total negative baryon density (1.4) in full field minimum-energy solutions.

Total negative baryon density (1.4) in the central tetrahedron as a function of m (integrating only over central tetrahedron).

Figure 6: $B = 3$ full field minimum-energy solutions data.

4.2. Expansion around the origin

The tetrahedral symmetry of the $B = 3$ Skyrme field poses stringent restrictions on the allowed terms in a Taylor expansion around the origin. Here we calculate the allowed polynomials and estimate the relevant coefficients from the numerical solution.

The rational map of the $B = 3$ Skyrmion is given by

$$R(z) = \frac{\sqrt{3}iz^2 - 1}{z^3 - \sqrt{3}iz} \tag{4.44}$$

which is T_d tetrahedrally symmetric using the same orientation as in [12]. This symmetry is generated by a C_2 symmetry

$$z \mapsto -z, \quad R \mapsto -R, \tag{4.45}$$

16

and a C_3 symmetry

$$z \mapsto \frac{iz+1}{-iz+1}, \quad R \mapsto \frac{-iR+i}{R+1}, \tag{4.46}$$

for the tetrahedral symmetry T, together with an additional reflection symmetry

$$z \mapsto \frac{\bar{z}-i}{-i\bar{z}+1}, \quad R \mapsto \frac{\bar{R}-i}{-i\bar{R}+1}. \tag{4.47}$$

The corresponding symmetries in component notation for the C_2 generator is

$$(x_1, x_2, x_3) \mapsto (-x_1, -x_2, x_3), \quad (\pi_1, \pi_2, \pi_3) \mapsto (-\pi_1, -\pi_2, \pi_3). \tag{4.48}$$

and

$$(x_1, x_2, x_3) \mapsto (x_2, x_3, x_1), \quad (\pi_1, \pi_2, \pi_3) \mapsto (\pi_3, \pi_1, \pi_2) \tag{4.49}$$

for the C_3 generator. The reflection symmetry is given by

$$(x_1, x_2, x_3) \mapsto (x_1, -x_3, -x_2), \quad (\pi_1, \pi_2, \pi_3) \mapsto (\pi_1, -\pi_3, -\pi_2) \tag{4.50}$$

Hence the field $\boldsymbol{\pi}$ can be expanded around the origin as

$$\boldsymbol{\pi} = a_1 \begin{pmatrix} x_1 \\ x_2 \\ x_3 \end{pmatrix} + b_1 \begin{pmatrix} x_2 x_3 \\ x_1 x_3 \\ x_1 x_2 \end{pmatrix} + c_1 \begin{pmatrix} x_1^3 \\ x_2^3 \\ x_3^3 \end{pmatrix} + c_2 r^2 \begin{pmatrix} x_1 \\ x_2 \\ x_3 \end{pmatrix}$$

$$+ d_1 \begin{pmatrix} x_2 x_3 x_1^2 \\ x_1 x_3 x_2^2 \\ x_1 x_2 x_3^2 \end{pmatrix} + d_2 r^2 \begin{pmatrix} x_2 x_3 \\ x_1 x_3 \\ x_1 x_2 \end{pmatrix} + \ldots, \tag{4.51}$$

where $r^2 = x_1^2 + x_2^2 + x_3^2$. The tetrahedral symmetry can be augmented to spherical symmetry by setting $b_1 = 0$, $c_1 = 0$ and $d_1 = d_2 = 0$, which corresponds to the Taylor expansion of the hedgehog ansatz around the origin. This provides a useful check that we have implemented the tetrahedral symmetry correctly.

In order to compare the Taylor expansion of $\boldsymbol{\pi}$ to the numerical solution, we have to calculate the coefficients in (4.51). We used the following approach. Setting $x_2 = 0$ and $x_3 = 0$ in (4.51) gives a polynomial in x_1. We fitted this polynomial to our numerical data using a least square fit, and this allows us to calculate a_1 and $c_1 + c_2$. Similarly, setting $x_2 = x_1$, and $x_3 = 0$ gives a_1, b_1, $c_1 + 2c_2$ and $2d_2$. Finally, setting $x_2 = x_1$ and $x_3 = x_1$ also gives an equation in d_1. In order to improve the approximation close to the origin, we fitted to a polynomial of higher degree. By plotting numerical data and approximation we found that the values $a_1 = -0.41$, $b_1 = -2.1$, $c_1 = -2.2$, $c_2 = 1.2$, $d_1 = 0.76$ and $d_2 = 0.64$ are a reasonable approximation for $-0.5 < x_1, x_2, x_3 < 0.5$. Note that the errors in particular for the coefficients d_1 and d_2 are rather large. We can now evaluate the Jacobian of the map. At the origin $\mathbf{x} = 0$, the Jacobian is non-zero, namely, $\det(J_0) = a_1^3 < 0$. The value of $\det J_0(0) = -0.055$ calculated numerically from the exact solution matches the value for the expansion (4.51).

Figure 7 shows a plot of the surface $\det J = 0$ inside a cube of length 0.5. This clearly looks very similar to the surface $\det J = 0$ arising from the numerical solution displayed in
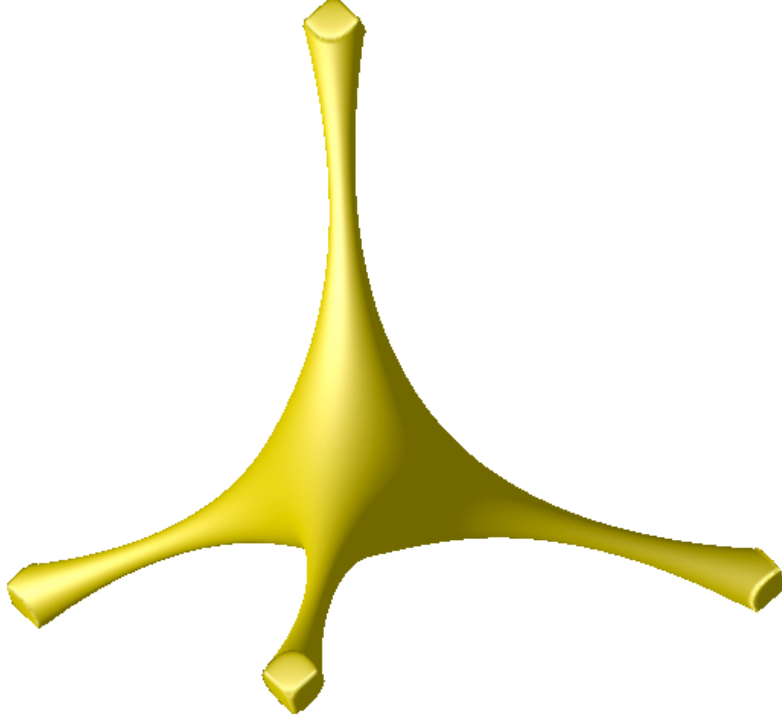
17

Figure 7: Singular surface $\det J = 0$ calculated using the polynomial expansion around the origin in (4.51). In this figure, $\det J = 0$ is displayed inside a cube of length 0.5.

figure 2b. Using our expansion, we can check whether the singular surface pinches off at a point. By setting $x_2 = x_1$, and $x_3 = x_1$ in the Jacobian J_0 we can show that $\det J_0 = 0$ for $x_1 = -0.09$ but there is no positive solution within the box. We were careful to include terms up to fourth order because the normal form of the swallowtail singularity is given by

$$
\begin{aligned}
y_1 &= x_1^4 + x_1^2 x_2 + x_1 x_3, \\
y_2 &= x_2, \\
y_3 &= x_3,
\end{aligned}
\tag{4.52}
$$

which includes a fourth order term. The Jacobian matrix of (4.52) is given by

$$
J = \begin{pmatrix} 4x_1^3 + 2x_1 x_2 + x_3 & x_1^2 & x_1 \\ 0 & 1 & 0 \\ 0 & 0 & 1 \end{pmatrix}.
\tag{4.53}
$$

The singular set $\det J = 0$ consists of folds, cusps and swallowtails and is given by $x_3 = -4x_1^3 - 2x_1 x_2$. The fold surfaces meet to form four cusp lines which in turn meet at the origin where the swallowtail is located.

In summary, we have deduced the following folding structure for the $B = 3$ Skyrmion. There are four folding tubes through the faces of a tetrahedron. These tubes smoothly connect to the corners of a dual tetrahedron at the origin. The folding surface are not intersecting each other, so there are no swallowtail singuarities in the $B = 3$ Skyrmion, contrary to

18

the conjecture in [11]. By symmetry, the cusp lines are expected to lie on the edges of the tetrahedron, and there is some numerical evidence.

5. Conclusion

This paper was motivated by the results of [11], where the authors found regions of negative baryon density in the rational maps for the $B = 3$ minimum-energy Skyrmion. For small m these regions of negative baryon density are very small, but we have been able to numerically verify their existence. Also we have discovered a tetrahedron of negative baryon density at the origin, which is dual to a tetrahedron produced as a level-surface of positive constant baryon density. The singularities corresponding to surfaces of zero baryon density form four tubes which smoothly join up at the dual tetrahedron at the origin. Contrary to the conjecture in [11], there are no swallowtail singularities in the $B = 3$ Skyrmion configuration. We have also found that for the $B = 3$ Skyrmion there are five pre-images of the anti-vacuum, four with positive orientation, on the vertices of a tetrahedron, and one with negative orientation at the origin. This behaviour is also seen in monopoles [23].

The authors of [11] did not find any regions of negative baryon density in the rational map ansatz for the $B = 4$ minimum-energy solution. This has been verified here numerically. Furthermore, assuming octahedral symmetry we have shown in appendix Appendix A that there are no regions of negative baryon density around the origin. These results are also consistent with the instanton ansatz [25].

It has already been discussed that regions of negative Jacobian-determinant occur for the charge three instanton [25]. This is significant because there is a BPS extended Skyrme model which can be derived from Yang-Mills instantons [26], which must contain regions of negative baryon density. This extended model has an infinite number of vector mesons. There has also been research into a truncated version of this model [27], where only a few extra terms are included. Understanding the form and distribution of the negative baryon density in these models would be very interesting. It should be noted that there is another BPS Skyrme model [28], where the Bogomolny equation shows that the baryon density is proportional to the square root of the potential. Hence, if the potential is positive definite through space, so is the baryon density.*

* This was pointed out by M. Speight.

Appendix A. $B = 4$

It has been shown [11] that even when the $B = 4$ rational map ansatz is extended to be non-holomorphic no negative baryon density is found. This is also seen in our full field minimisation of the $B = 4$ Skyrmion for $m = 0$ and $m = 1$, see figure A1a and A1b, respectively. For $m = 0$ we found $E/B = 1.12$, and for $m = 1$ we found $E/B = 1.30$. In both cases, up to numerical accuracy, we did not find any negative baryon density.

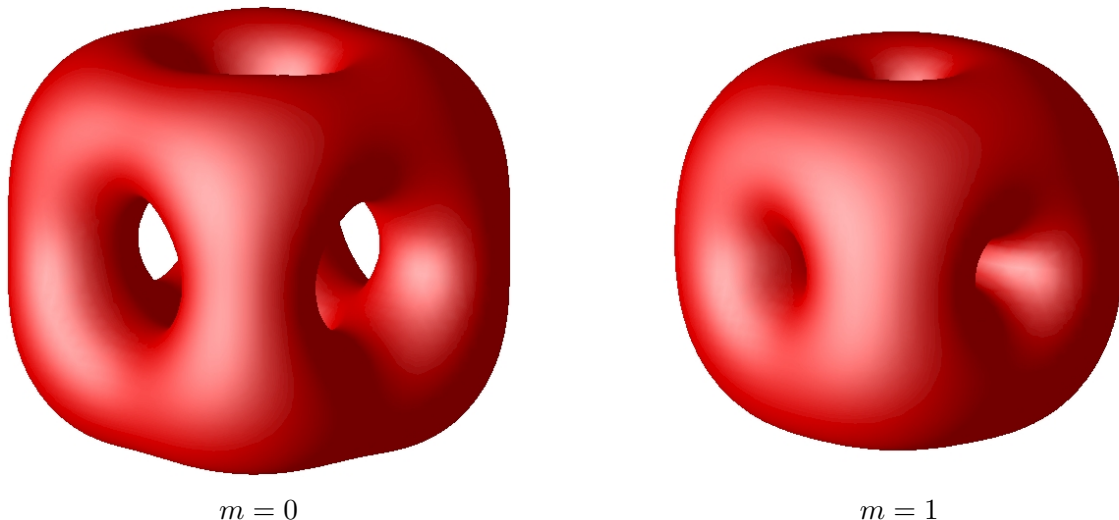$m = 0$ $\qquad\qquad\qquad\qquad\qquad\qquad$ $m = 1$

Figure A1: Minimum-energy full field solutions of the $B = 4$ Skyrmion. Red is a surface of constant positive $\det(J)$.

In the following, we show that the $B = 4$ minimum-energy octahedrally symmetric Skyrmion does not have regions of negative baryon density near the origin. This is where the non-holomorphic rational map ansatz is not a good approximation of the exact solution. As a starting point, we consider the rational map of the $B = 4$ Skyrmion is given by

$$R(z) = \frac{z^4 + 2\sqrt{3}iz^2 + 1}{z^4 - 2\sqrt{3}iz^2 + 1} \tag{A.1}$$

which is octahedrally symmetric. This symmetry is generated by a C_4 symmetry:

$$z \mapsto iz, \quad R \mapsto \frac{1}{R}, \tag{A.2}$$

and a C_3 symmetry

$$z \mapsto \frac{iz + 1}{-iz + 1}, \quad R \mapsto e^{-\frac{2\pi i}{3}}R. \tag{A.3}$$

The corresponding symmetries in component notation for the C_4 generator is

$$(x_1, x_2, x_3) \mapsto (x_2, -x_1, x_3), \quad (\pi_1, \pi_2, \pi_3) \mapsto (\pi_1, -\pi_2, -\pi_3). \tag{A.4}$$

and

$$(x_1, x_2, x_3) \mapsto (x_2, x_3, x_1), \quad (\pi_1, \pi_2, \pi_3) \mapsto \left(-\frac{1}{2}\pi_1 - \frac{1}{2}\sqrt{3}\pi_2, \frac{1}{2}\sqrt{3}\pi_1 - \frac{1}{2}\pi_2, \pi_3\right) \text{(A.5)}$$

for the C_3 generator. Hence the field $\boldsymbol{\pi}$ can be expanded around the origin as

$$\boldsymbol{\pi} = b_1 \begin{pmatrix} x_1^2 + x_2^2 - 2x_3^2 \\ -\sqrt{3}x_1^2 + \sqrt{3}x_2^2 \\ 0 \end{pmatrix} + c_1 \begin{pmatrix} 0 \\ 0 \\ x_1 x_2 x_3 \end{pmatrix}$$
$$+ d_1 \begin{pmatrix} x_1^4 + x_2^4 - 2x_3^4 \\ -\sqrt{3}x_1^4 + \sqrt{3}x_2^4 \\ 0 \end{pmatrix} + d_2 \begin{pmatrix} 2x_1^2 x_2^2 - x_1^2 x_3^2 - x_2^2 x_3^2 \\ -\sqrt{3}x_1^2 x_3^2 + \sqrt{3}x_2^2 x_3^2 \\ 0 \end{pmatrix} + \dots$$

A similar expansion as r tends to infinity has been performed in [22]. We can now evaluate the Jacobian of the map. At the origin $\mathbf{x} = 0$, the Jacobian is identically zero. Hence the singularity is clearly non-generic since for a generic singularity the Jacobian has rank 2. The determinant of the Jacobian can be expanded into $O-$symmetric polynomials. The lowest order term is

$$\det(J) = \sqrt{3}b_1^2 c_1 \left(x_1^2 x_2^2 + x_2^2 x_3^2 + x_3^2 x_1^2\right) + \dots$$

Hence the singularities are on the three coordinate axes which meet at the origin. Furthermore, sufficiently close to the origin $\det(J)$ is positive, and hence there is no negative baryon density.

References

[1] T.H.R. Skyrme. A Nonlinear field theory. Proc.Roy.Soc.Lond., A260:127–138, 1961.

[2] Edward Witten. Global Aspects of Current Algebra. Nucl.Phys., B223:422–432, 1983.

[3] Richard A. Battye, Nicholas S. Manton, Paul M. Sutcliffe, and Stephen W. Wood. Light Nuclei of Even Mass Number in the Skyrme Model. Phys.Rev., C80:034323, 2009.

[4] F. Meier and H. Walliser. Quantum corrections to baryon properties in chiral soliton models. Phys.Rept., 289:383–450, 1997.

[5] F.G. Scholtz, B. Schwesinger, H.B. Geyer. The Casimir energy of strongly bound B = 2 configurations in the Skyrme model. Nucl.Phys.A, 561:542, 1993.

[6] Gregory S. Adkins, Chiara R. Nappi, and Edward Witten. Static Properties of Nucleons in the Skyrme Model. Nucl.Phys., B228:552, 1983.

[7] Gregory S. Adkins and Chiara R. Nappi. The Skyrme Model with Pion Masses. Nucl.Phys., B233:109, 1984.

[8] Richard A. Battye, Steffen Krusch, and Paul M. Sutcliffe. Spinning skyrmions and the skyrme parameters. Phys.Lett., B626:120–126, 2005.

[9] Nicholas S. Manton and Stephen W. Wood. Reparametrising the Skyrme model using the lithium-6 nucleus. Phys.Rev., D74:125017, 2006.

[10] N.S. Manton. Geometry of Skyrmions. Commun.Math.Phys., 111:469, 1987.

[11] Conor J. Houghton and Steffen Krusch. Folding in the Skyrme model. J.Math.Phys., 42:4079–4100, 2001.

[12] Conor J. Houghton, Nicholas S. Manton, and Paul M. Sutcliffe. Rational maps, monopoles and Skyrmions. Nucl.Phys., B510:507–537, 1998.

[13] S. Krusch. S**3 skyrmions and the rational map ansatz. <u>Nonlinearity</u>, 13:2163, 2000.

[14] Steffen Krusch. Fermions coupled to skyrmions on S**3. <u>J.Phys.</u>, A36:8141, 2003.

[15] N.S. Manton and P. Sutcliffe. <u>Topological solitons</u>. Cambridge Monographs on Mathematical Physics. Cambridge University Press, 2004.

[16] Richard A. Battye and Paul M. Sutcliffe. Skyrmions, fullerenes and rational maps. <u>Rev.Math.Phys.</u>, 14:29–86, 2002.

[17] Steffen Krusch. Homotopy of rational maps and the quantization of skyrmions. <u>Annals Phys.</u>, 304:103–127, 2003.

[18] Richard A. Battye, Conor J. Houghton, and Paul M. Sutcliffe. Icosahedral skyrmions. <u>J.Math.Phys.</u>, 44:3543–3554, 2003.

[19] Richard A. Battye and Paul M. Sutcliffe. Symmetric skyrmions. <u>Phys.Rev.Lett.</u>, 79:363–366, 1997.

[20] Eric Braaten, Steve Townsend, and Larry Carson. Novel Structure of Static Multi - Soliton Solutions in the Skyrme Model. <u>Phys.Lett.</u>, B235:147, 1990.

[21] N.S. Manton. Skyrmions and their pion multipole moments. <u>Acta Phys.Polon.</u>, B25:1757–1764, 1994.

[22] Dankrad T.J. Feist. Interactions of B = 4 Skyrmions. <u>JHEP</u>, 1202:100, 2012.

[23] Paul M. Sutcliffe. Monopole zeros. <u>Phys.Lett.</u>, B376:103–110, 1996.

[24] Richard Battye and Paul Sutcliffe. Skyrmions and the pion mass. <u>Nucl.Phys.</u>, B705:384–400, 2005.

[25] R.A. Leese and N.S. Manton. Stable instanton generated Skyrme fields with baryon numbers three and four. <u>Nucl.Phys.</u>, A572:575–599, 1994.

[26] Paul Sutcliffe. Skyrmions, instantons and holography. <u>JHEP</u>, 1008:019, 2010.

[27] Paul Sutcliffe. Skyrmions in a truncated BPS theory. <u>JHEP</u>, 1104:045, 2011.

[28] C. Adam, C.D. Fosco, J.M. Queiruga, J. Sanchez-Guillen, and A. Wereszczynski. Symmetries and exact solutions of the BPS Skyrme model. <u>J.Phys.</u>, A46:135401, 2013.